UNIVERSIDADE DE SÃO PAULO

INSTITUTO DE FÍSICA
CAIXA POSTAL 20516
01498 - SÃO PAULO - SP
BRASIL

publicações

IFUSP/P-451

THE ^{10,11}B(p,n)^{10,11}C REACTIONS BETWEEN E_p = 13.6 AND 14.7 MEV

by

H.R. Schelin, E. Farrelly Pessoa, W.R. Wylie, J.L. Cardoso Jr. and R.A. Douglas

Instituto de Física, Universidade de São Paulo

Janeiro/1984

THE $^{10,11}B(p,n)\ ^{10,11}C$ REACTIONS BETWEEN $E_p = 13.6$ AND 14.7 MeV

H.R. Schelin*, E. Farrelly Pessoa, W.R. Wylie*,
J.L. Cardoso Jr.* and R.A. Douglas**

Departamento de Física Nuclear, Instituto de Física,
Universidade de São Paulo, CP 20516, 01498 São Paulo, SP, Brasil

ABSTRACT

Absolute differential cross sections for the n_0 and n_1 neutron groups for the reaction $^{10}B(p,n)\ ^{10}C$ and the n_0, n_1, n_2, n_3, n_4+n_5, n_6 and n_7 neutron groups for the reaction $^{11}B(p,n)\ ^{11}C$ have been measured at incident proton energies of 14.0, 14.3 and 14.6 MeV in the angular interval 20^0 to 160^0 along with excitation curves at $\theta_{lab} = 30^0$ from $E_p = 13.6$ to 14.7 MeV.

NUCLEAR REACTIONS: $^{10,11}B(p,n)\ ^{10,11}C$, E_p = 14.0, 14.3 and 14.6 MeV measured $\sigma(E_d,\theta)$ and excitation functions at $\theta_{lab} = 30^0$ for $E_p = 13.6$ to 14.7 MeV. Seven neutron groups observed for ^{11}B and two neutron groups for ^{10}B using time-of-flight techniques.

*Centro Técnico Aeroespacial, IEAv/FEX, Caixa Postal 6044, 12200 - S.J. Campos, SP, Brasil

**Departamento de Física Aplicada, IFGW, Universidade Estadual de Campinas, São Paulo, Brasil.

1. INTRODUCTION

Recent interest in proton induced reactions on p-shell target nuclei has appeared in the literature[1]. The direct interaction mechanism contributing to these reactions is considered to be a microscopic interaction, represented by the Bersch[2] g-matrix interaction, within the framework of a Distorted Wave Born Approximation. Reductions in the g-matrix interaction strengths are estimated by comparison of the calculated cross sections with the experimental values.

In view of this revival of interest in p-shell nuclei we have measured the differential cross sections for the reactions $^{10,11}B(p,n)^{10,11}C$ at incident proton energies in the region E_p = 13.7 - 14.7 MeV.

2. EXPERIMENTAL PROCEDURE

The pulsed proton beam of the University of São Paulo Pelletron Accelerator was used to study the reactions $^{10}B(p,n)^{10}C$ and $^{11}B(p,n)^{11}C$ in the energy region E_p = 13.7 to 14.7 MeV. Neutron detection employed conventional time of flight techniques. Detailed descriptions of the beam pulsing system, the experimental arrangement and the electronics associated with the time of flight system may be found in references 3 and 4.

In the present work, the average on target intensity of the proton beam was about 90 nanoamps. The time resolution of the system, obtained from the FWHM of the target gamma ray peak was 1.5 - 2 nanoseconds. The ratio of beam current collected on a $\emptyset$ = 5 mm collimator located 7 cm upstream from the target,

to the on-target beam current was of the order 1:200 . A flight path of 4.0 meters was used in obtaining all of the spectra. The neutrons were detected in a NE 213 liquid scintillator, with dimensions $\emptyset$ = 12.7 cm , ℓ = 2.54 cm, optically coupled to a RTC 58 AVP photomultiplier. Pulse shape discrimination, used to differentiate the gamma from the neutron events, allowed about 90% of the gamma events to be eliminated from the spectra without incurring any neutron loss.

The neutron detection efficiency of the NE 213 scintillator was calculated using a Monte Carlo computer code[5]. The detection threshold was selected for 2.2 MeV neutron energy. In equivalent electron energy, this corresponds to the compton edge of the 661 keV gamma from ^{137}Cs .

The targets were mounted in a low mass scattering chamber which minimized neutron absorption and scattering. The beam stop consisted of a Faraday cup situated 1.5 meters downstream from the target and shielded by a hollow lead box which contained water. Target monitoring was performed by counting neutron events, within a predetermined energy window, which occurred in a small NE 111 plastic scintillator placed close to the target at 90^0 to the beam direction.

The Boron targets were made by centrifuging a colloidal suspension of the enriched isotope onto a mylar film[6,7,8]. In this process a small amount of the colloid is deposited along with the isotope. In order to determine the nature of the neutron spectra associated with the colloid and mylar, a set of "background targets" were prepared in a similar manner, the sole difference being the omission of the Boron in the suspension. The thicknesses and uniformities of the targets were determined by measuring the energy loss incurred during the passage through

the target of a 5.0 MeV alpha particle from ^{241}Am . The uncertainties in target thickness due to non uniformities are of the order of 10% . Table I gives a résume of the characteristics of the targets used in the present work.

The neutron spectra were stored in a Honeywell DDP-516 "on-line" computer and subsequently recorded on magnetic tape via an IBM 360/44.

3. ANALYSIS OF THE SPECTRA

Neutron spectra were measured for the reactions $^{10}B(p,n)^{10}C$ and $^{11}B(p,n)^{11}C$ in order to obtain angular distributions at E_p = 14.0, 14.3 and 14.6 MeV and excitation functions in the energy interval E_p = 13.7 to 14.7 MeV at $\theta_{lab} = 30^0$.

Figure 1 shows spectra, typical for the reaction $^{11}B(p,n)^{11}C$, measured at E_p = 14.7 MeV , $\theta_{lab} = 30^0$ and at E_p = 14.6 MeV , $\theta_{lab} = 100^0$. Peak identifications made on the basis of kinematic calculation and associated flight times show the presence of neutrons groups which leave the residual nucleus ^{11}C in the ground state (n_0) and the first eleven excited states n_1 , n_2 , n_3 , $n_4 + n_5$ (unresolved), n_6 , n_7 , n_8 , n_9 , and $n_{10} + n_{11}$ (unresolved).

Figure 2 shows spectra, typical for the reaction $^{10}B(p,n)^{10}C$, measured at E_p = 14.7 MeV , $\theta_{lab} = 30^0$ and E_p = 14.6 MeV , $\theta_{lab} = 100^0$. For this case, neutron groups are identified which leave the residual nucleus ^{10}C in the ground state (n_0) and the first excited state (n_1). Figure 3 is a diagram of the energy levels in $^{10,11}C$ which are associated

with the observed neutron groups.

The enriched isotope of ^{10}B contains about 10% of ^{11}B "contamination". Since the cross sections for the $^{11}B(p,n)^{11}C$ reactions are considerably larger than the $^{10}B(p,n)^{10}C$ ones, neutron peaks arising from the ^{11}B reactions appear with appreciable intensity in the ^{10}B spectra. In addition, the kinematics of the two reactions are such that, although the n_0 neutron group of the ^{11}B reaction is an isolated peak, the n_1 and n_3 groups from ^{11}B overlap respectively the n_0 and n_1 groups from ^{10}B, especially at the forward angles. A proper analysis of the $^{10}B(p,b)^{10}C$ spectra requires a subtraction of the ^{11}B neutrons.

This was accomplished by measuring the $^{11}B(p,n)^{11}C$ enriched isotope spectra at the same incident proton energies and laboratory angles as the $^{10}B(p,n)^{10}C$ data, thus obtaining pairs of neutron spectra for the two isotopes. For each pair a ratio of the peak area of the ^{11}B n_0-group was obtained to provide a normalization factor for the total $^{11}B(p,n)^{11}C$ spectrum which, after such normalization, was superimposed on the $^{10}B(p,n)^{10}C$ spectrum for correction.

Figures 1 and 2 also reveal a continuous neutron background which was subtracted during the analysis of the neutron peaks. In order to investigate the source of this background, spectra were measured for a target consisting of the collodian + mylar backing. Such "background" spectra are illustrated in figure 4 for two laboratory angles, $\theta_{lab} = 30^0$ and 90^0, at $E_p = 14.0$ MeV. These give full account of the continuum observed in the Boron spectra. In addition, targetless spectra were measured which showed a negligible neutron intensity.

A small portion of gamma rays are also present in

the spectra in the form of two distinct peaks, which correspond to target gammas and beam stop gammas. These were purposely admitted by the n/γ differentiation system since the target gamma peak position was needed for the kinematic identification of the neutron groups and the energy transform of the time-of-flight spectra.

Figure 5 show transforms of the time-of-flight spectra, shown in figures 1a and 2a to energy spectra i.e. $N(E)\,dE$ versus channel. These transforms were calculated for a constant energy bin of $\Delta E = 60$ keV, a value which approximates the target thicknesses used in the experiment.

The areas of the neutron peaks in the Boron spectra were determined with a peak-fit computer code[9] which adjusted the shapes of the peaks by a function composed of a mixture of Gaussian and Lorentzian distributions. Asymmetries in the shapes were taken into account by including in the function the derivative of a gaussian curve. The program also adjusted the background under the peaks to a parabolic function which was subsequently subtracted. The areas were calculated by the standard procedure of minimizing χ^2.

4. THE DIFFERENTIAL CROSS SECTIONS

Laboratory differential cross sections were calculated using the formula

$$\left(\frac{d\sigma}{d\Omega}\right)_{lab} = \frac{Y}{n\,N\,\varepsilon(E_n)\,d\Omega}$$

where Y is the neutron yield or spectral peak area per beam

charge integration, n is the number of incident particles per charge integration, N is the number of target nuclei/unit area, $\varepsilon(E_n)$ is the neutron detection efficiency at neutron energy E_n, and $d\Omega$ is the solid angle subtended by the neutron detector.

The laboratory differential cross sections were transformed to center of mass differential cross sections by standard computer codes.

Figure 6 is a set of excitation curves for the n_0, n_1, n_2, n_3, $n_4 + n_5$, n_6 and n_7 neutron groups from the reaction $^{11}B(p,n)^{11}C$ obtained at $\theta_{lab} = 30^0$ in the incident energy interval between E_p = 13.7 to 14.7 MeV taken in 100 keV increments. Figure 7 shows the excitation curves for the n_0 and n_1 groups from the reaction $^{10}B(p,n)^{10}C$ in the same incident energy interval and laboratory angle as described for figure 6. Figure 8 shows center of mass angular distributions obtained in the angular interval $\theta_{CM} = 20^0$ to 160^0 at E_p = 14.0, 14.3 and 14.6 MeV for each of the neutron groups n_0, n_1, n_2, n_3, $(n_4 + n_5)$, n_6 and n_7 from the reaction $^{11}B(p,n)^{11}C$. Figure 9 shows angular distributions at the same incident energies and angular interval for the n_0 and n_1 neutron groups from the reaction $^{10}B(p,n)^{10}C$.

We mention that although the n_8, n_9 and $(n_{10} + n_{11})$ neutron groups appear in the spectrum of fig. 1, an analysis of these groups to obtain their angular distributions was not possible. This is because the neutron detection threshold (2.2 MeV) was too high in these measurements to obtain reliable yields for these neutron groups at the other laboratory angles.

5. UNCERTAINTIES

The uncertainties associated with the differential cross section arise from the following sources.

a) The determination of the neutron peak areas (yields) contribute 1 - 10%.

b) The estimation of the target thickness and uniformities introduced about 10%.

c) The precision of the charge integration circuit which determined the number of incident particles may be considered < 5%.

d) The uncertainties associated with the determination of the detector solid angle are less than 1%.

e) The calculated neutron detection efficiencies contribute 5 - 8%.

The totality of the uncertainties from the various sources result in an overall uncertainty of 12 - 17% for the differential cross sections.

6. DISCUSSION

A résume of differential cross section measurements reported in the literature for the $^{10,11}B(p,n)^{10,11}C$ reactions is given in table 2. The references have been organized according to the incident proton energy, the neutron detection techniques employed, the type of data (angular distribution or excitation curve) presented for a given neutron group and pertinent details concerning the cross section values.

The principal works existing for the $^{10}B(p,n)^{10}C$

reaction are those of references 10, 11 and 12 of table 2. Ajzenberg and Franzen[10] used proton recoil techniques to measure angular distributions for the n_0 and n_1 neutron groups at E_p = 17.2 MeV for five angles between $\theta_{cm} = 30^0$ and 150^0. Their cross section values, however, were reported in relative units which prevents comparison with our magnitudes although good agreement in shape exists between their angular distributions and ours. Goodman et al.[11] used time-of-flight techniques to measure two angular distributions for the n_0 group at E_p = 16 and 23 MeV, between $\theta_{cm} = 10^0$ and 150^0. Due to their presentation of cross sections in relative units, once again, no comparison of magnitudes could be made although good agreement in shape was obtained. Clough et al.[12] using time-of-flight techniques reported angular distributions in units of mb/sr at E_p = 30 and 50 MeV for the n_0, n_1 and n_2 neutron groups. Although their incident proton energies are a good deal higher than those of the present work, their cross sections are close in magnitude. For example at $\theta_{lab} = 30^0$, their E_p = 30 MeV cross section is the same as our E_p = 14.6 MeV value (0.2 mb/sr) for the n_0 group and about 50% higher than our value (0.5 mb/sr) for the n_1 group.

In all three works cited above, no mention is made of possible contamination of the $^{10}B(p,n)^{10}C$ spectra by the presence of ^{11}B in the target. In the present work we found that correction for such contamination was extremely important and for this reason for each $^{10}B(p,n)^{10}C$ spectra obtained, a comparison spectrum at the same incident proton energy and detector angle was measured for the $^{11}B(p,n)^{11}$ reaction. This procedure was necessary even when the ^{10}B targets were of the enriched isotope.

The principal works existing for the $^{11}B(p,n)^{11}C$ reaction are those of references 11 - 17 in table 2. We shall limit our discussion to a comparison with those measurements which also employed time of flight techniques and for which the incident proton energies are closest to our region of about 14.3 MeV. Overley and Borchers[15] present a very extensive work in which they report differential cross sections in mb/sr for twenty five angular distributions plus excitation curves at $\theta_{lab} = 0$ and 90^0 for the n_0, n_1, n_2 and n_3 neutron groups. For the n_0 neutron group the excitation curves measured in the incident energy interval E_p = 4.0 to 11.5 MeV show many broad fluctuations indicating the presence of compound nucleus formation. At $\theta_{lab} = 90^0$ and E_p = 11.5 MeV they report a cross section value of about 6 mb/sr as compared to our value at $\theta_{lab} = 90^0$ and E_p = 14.0 MeV of 1.1 mb/sr. Thus at an energy about 2.5 MeV beyond their last measured point the cross section has dropped by a factor of six. This seemed a rather abrupt change. However, the works of J.D. Anderson et al.[16,17] report angular distributions in mb/sr at E_p = 17 and 18 MeV for the n_0 and n_1 groups and a second set of angular distributions at E_p = 18 MeV for the n_0, n_1, n_2 and n_3 neutron groups. Comparison of their cross sections for all these four neutron groups agrees extremely well both in shape and magnitude with those of the present work at E_p = 14.6 MeV, showing that there is indeed a sharp dropping off of the Overley and Borchers measurements at higher incident energies.

Reports of differential cross sections for the neutron groups n_4 through n_7, leading to higher excited states in ^{11}C were not found in the literature. Thus no basis for comparison of our values for these neutron groups is available at present.

ACKNOWLEDGEMENTS

The authors wish to thank Prof. O. Sala for providing the Pelletron facilities, C.M. Figueiredo and L.M. Fagundes for the technical assistance they offered during the data taking, J.D. Rogers and A. Peterlevitz of UNICAMP for furnishing the peak fit computer codes used in the present work and Prof. A. Galonsky of Michigan State University who suggested this experiment. We would also like to acknowledge the financial aid extended to us by CNPq and FINEP.

REFERENCES

1. F. Petrovich, R.H. Howell, C.H. Poppe, S.M. Austin and G.M. Crawley, Nuclear Physics A383 (1982) 355.
2. G. Bertsch, J. Borysowicz, H. McManus, W.G. Love, Nuclear Physics A284 (1977) 390.
3. W.R. Wylie, E. Farrelly Pessoa, E.W. Cybulska, H.R. Schelin, L.M. Fagundes, K. Nakayama and R.A. Douglas, Nucl. Instr. 164 (1979) 293.
4. H.R. Schelin (Master's Thesis) 1979, Departamento de Física Nuclear, Universidade de São Paulo.
5. K. Nakayama, E. Farrelly Pessoa and R.A. Douglas, Nucl. Instr. 190 (1981) 555.
6. J.P. Richaud, Nucl. Instr. 167 (1979) 97.
7. I. Sugai, Nucl. Instr. 145 (1977) 409.
8. R. Liguori Neto and P.R.S. Gomes, Relatório de Atividades (1982), Departamento de Física Nuclear, Universidade de São Paulo, pg. 45 .
9. J.D. Rogers, Universidade Estadual de Campinas, (Private Communication).
10. F. Ajzenberg and W. Franzen, Phys. Rev. 95 (1954) 1531.
11. C.D. Goodman, H.W. Fielding and D.A. Lind, Technical Progress Report (1973) University of Colorado.
12. A.S. Clough, C.J. Batty, B.E. Bonner and L.E. Williams, Nucl. Phys. A143 (1970) 385.
13. K. Hisatake, Y. Ishizak, A. Isoya, T. Nakamura, Y. Nakano, B. Saheki, Y. Suji, K. Yuasa, J. Phys. Soc. Japan 15 (1960) 741.
14. R.D. Albert, S.D. Bloom and N.K. Glendenning, Phys. Rev. 122 (1961) 862.

15. J.C. Overley and R.R. Borchers, Nucl. Phys. 65 (1965) 156.

16. J.D. Anderson, C. Wong, J.W. McClure and B.D. Walker, Phys. Rev. 136B (1964) 118.

17. J.D. Anderson, Nucl. Spectrosc. and React. Pt. B, 613 (1974).

TABLE CAPTIONS

Table I - Characteristics of the targets used in the present work.

Table II - Previous measurements of the $^{10,11}B(p,n)^{10,11}C$ reactions.

FIGURES CAPTIONS

Fig. 1 - Typical spectra for the $^{11}B(p,n)^{11}C$ reaction.
1a) $\theta_{lab} = 30^0$ and $E_p = 14.7$ MeV. 1b) $\theta_{lab} = 100^0$ and $E_p = 14.6$ MeV.

Fig. 2 - Typical spectra for the $^{10}B(p,n)^{10}C$ reaction.
2a) $\theta_{lab} = 30^0$ and $E_p = 14.7$ MeV. 2b) $\theta_{lab} = 100^0$ and $E_p = 14.6$ MeV.

Fig. 3 - Energy diagrams for the levels observed in $^{10,11}C$.

Fig. 4 - Typical spectra for the collodion plus mylar target.
4a) $\theta_{lab} = 30^0$ and $E_p = 14.0$ MeV. 4b) $\theta_{lab} = 90^0$ and $E_p = 14.0$ MeV.

Fig. 5 - Energy transform of the time-of-flight spectra.
5a) $^{11}B(p,n)^{11}C$ reaction at $\theta_{lab} = 30^0$ and $E_p = 14.7$ MeV.
5b) $^{10}B(p,n)^{10}C$ reaction at $\theta_{lab} = 30^0$ and $E_p = 14.7$ MeV.

Fig. 6 - Excitation curves for neutron groups from the reaction $^{11}B(p,n)^{11}C$ at $\theta_{lab} = 30^0$.

Fig. 7 - Excitations curves for neutron groups from the reaction $^{10}B(p,n)^{10}C$ at $\theta_{lab} = 30^0$.

Fig. 8 - Angular distributions at $E_p = 14.0$, 14.3 and 14.6 MeV for neutron groups from the reaction $^{11}B(p,n)^{11}C$.

Fig. 9 - Angular distributions at $E_p = 14.0$, 14.3 and 14.6 MeV for neutron groups from the reaction $^{10}B(p,n)^{10}C$.

TABLE I

E_p (MeV)	Target	Thickness (mg/cm^2)	Thickness (keV)	Nº of nuclei of B/cm^2
14.0*	^{10}B	1.84 ± 10%	71.8	111×10^{18}
	^{11}B	2.40 ± 10%	93.6	131×10^{18}
13.6** a 14.6	^{10}B	1.24 ± 10%	48.4	74.6×10^{18}
	^{11}B	2.89 ± 10%	112.7	158×10^{18}

*Targets used in the angular distributions at $E_p = 14.0$ MeV.

**Targets used in the angular distributions at $E_p = 14.3$ and 14.6 MeV and in the excitation curves from $E_p = 13.6$ to 14.7 MeV.

TABLE II

Reaction	Energy (MeV)	Detection Technique	Measured	Ref.	OBS.
$^{10}B(p,n)^{10}C$	17.2	Method of proton recoils in thick photographic emulsions	1 A.D. for n_0 and n_1	(10)	Cross sections in relative units
$^{10}B(p,n)^{10}C$ and $^{11}B(p,n)^{11}C$	16 and 23	Time-of-flight liquid scintillator	2 A.D. for $^{10}B(p,n)^{10}C(n_0)$ and 2 A.D. for $^{11}B(p,n)^{11}C$ (n_0 and n_3)	(11)	Cross sections in relative units
$^{10}B(p,n)^{10}C$ and $^{11}B(p,n)^{11}C$	30 and 50	Time-of-flight liquid scintillator	2 A.D. for $^{10}B(p,n)^{10}C$ (n_0, n_1 and n_2) and 2 A.D. for $^{11}B(p,n)^{11}C$ (n_0, n_1 and $n_2 + n_3$)	(12)	Cross sections in mb/sr; θ_{cm} between 0 and 60^0
$^{11}B(p,n)^{11}C$	8.1 to 14.1	Proton recoil fast neutron spectrometer	5 A.D. for n_0	(13)	Cross sections in mb/sr
$^{11}B(p,n)^{11}C$	2.9 to 4.3	Long-counter detection technique	10 A.D. for n_0	(14)	Cross sections in relative units
$^{11}B(p,n)^{11}C$	4.0 to 11.5	Time-of-flight plastic scintillator	1 E.C. 25 A.D. for n_0, n_1, n_2 and n_3	(15)	Cross section in mb/sr
$^{11}B(p,n)^{11}C$	17 to 18	Time-of-flight plastic scintillator	2 A.D. for n_0 and n_1	(16)	Cross sections in mb/sr
$^{11}B(p,n)^{11}C$	18	Time-of-flight	1 A.D. for n_0, n_1, n_2 and n_3	(17)	Cross sections in mb/sr

A.D. = Angular distribution.

E.C. = Excitation curve.

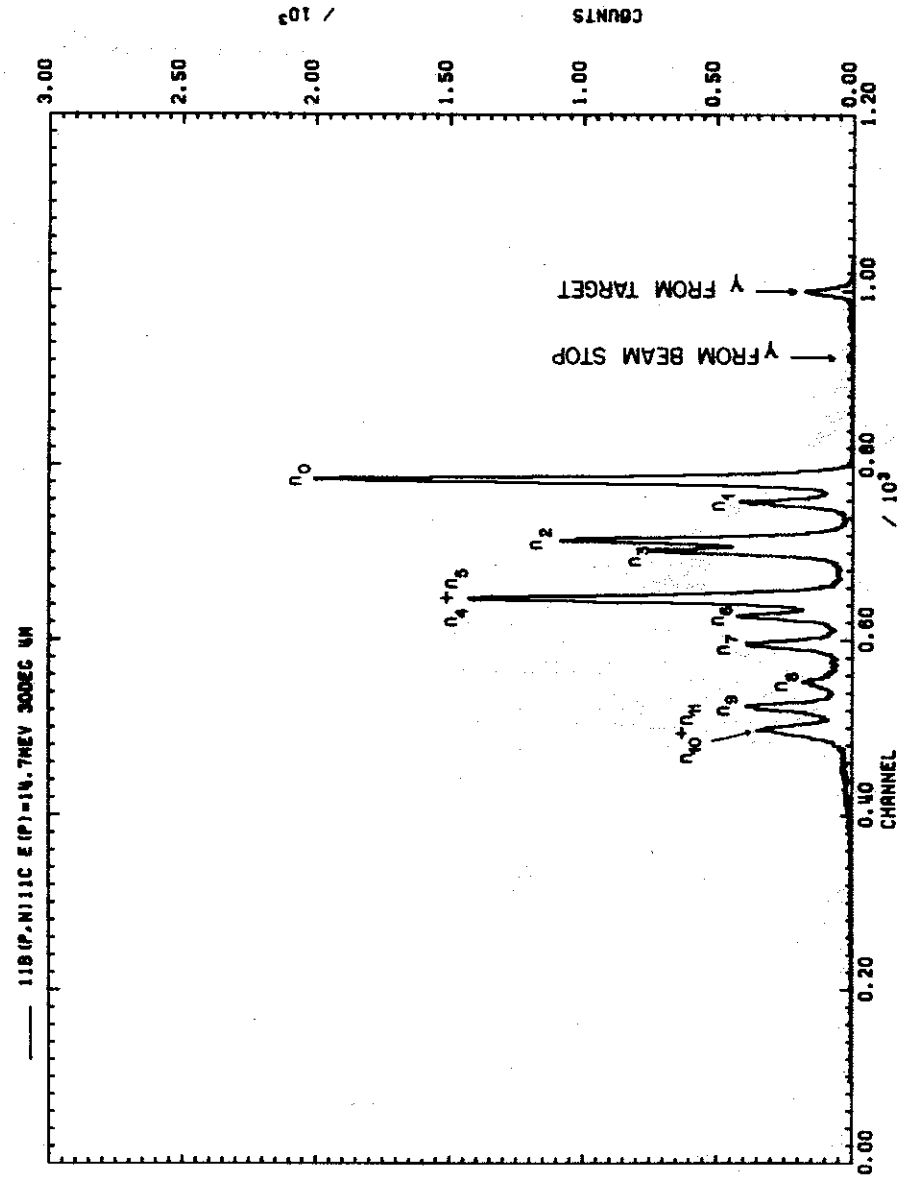

Fig. 1a

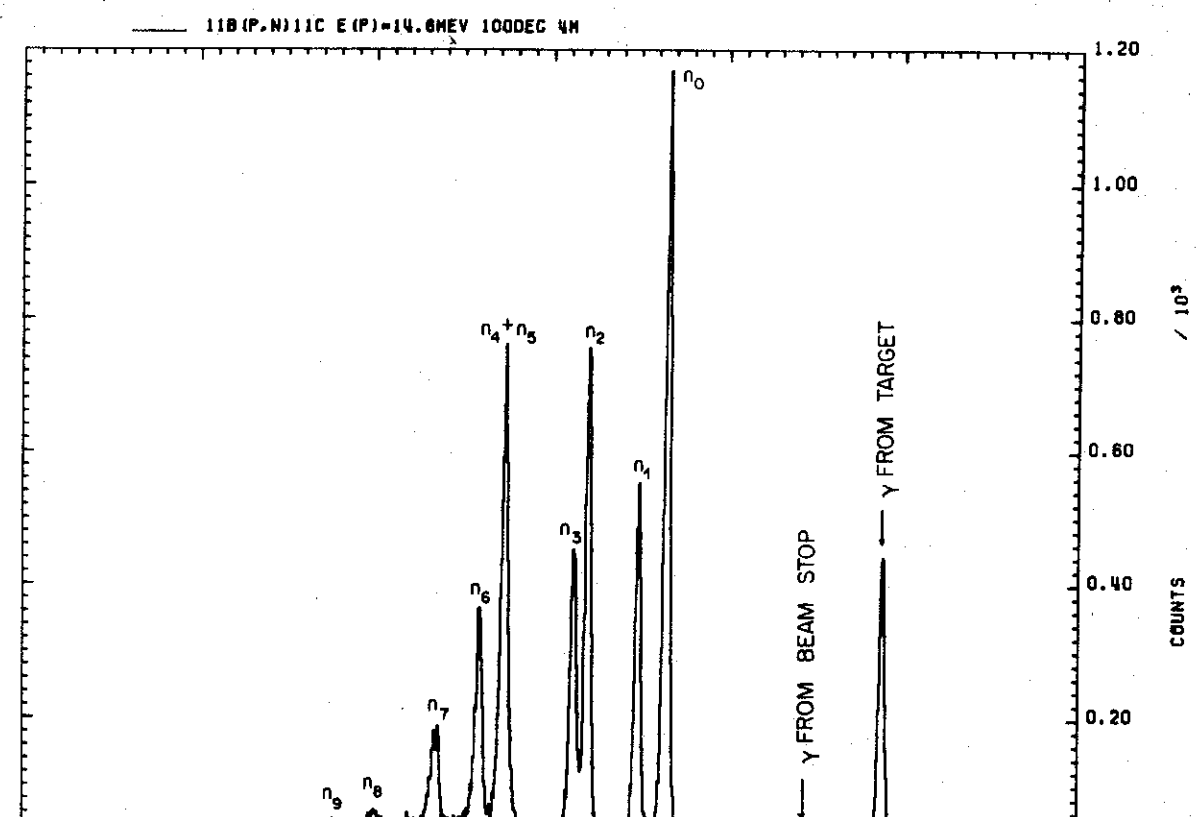
11B(P,N)11C E(P)=14.6MEV 100DEG 4M
n0
n1
n2
n3
n4+n5
n6
n7
n8
n9
γ FROM BEAM STOP
γ FROM TARGET
CHANNEL
/ 10³
COUNTS
/ 10³
0.00
0.20
0.40
0.60
0.80
1.00
1.20

Fig. 1b

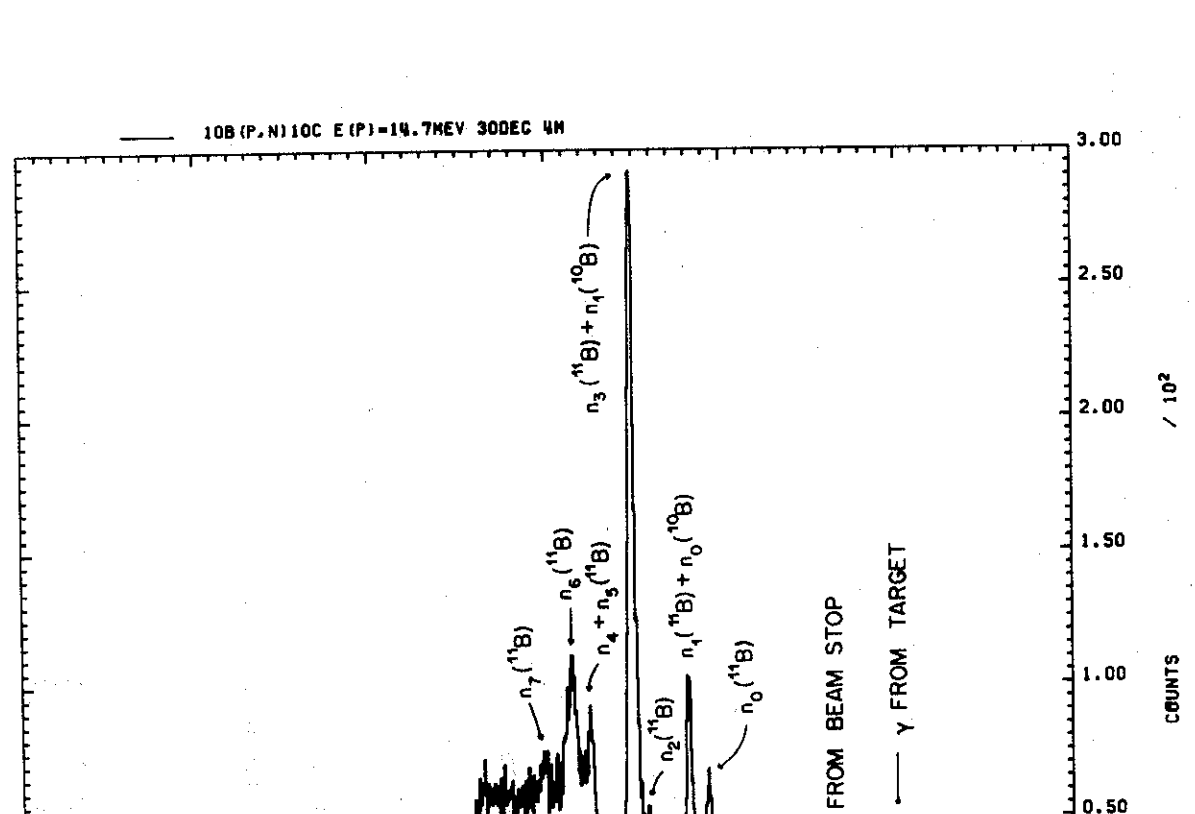
10B(P,N)10C E(P)=14.7MEV 300DEG 4M
n3(11B)+n1(10B)
n6(11B)
n4+n5(11B)
n7(11B)
n2(11B)
n1(11B)+n0(10B)
n0(11B)
γ FROM BEAM STOP
γ FROM TARGET
CHANNEL
/ 10³
COUNTS
/ 10²
0.00
0.20
0.40
0.60
0.80
1.00
1.20
0.50
1.50
2.00
2.50
3.00

Fig. 2a

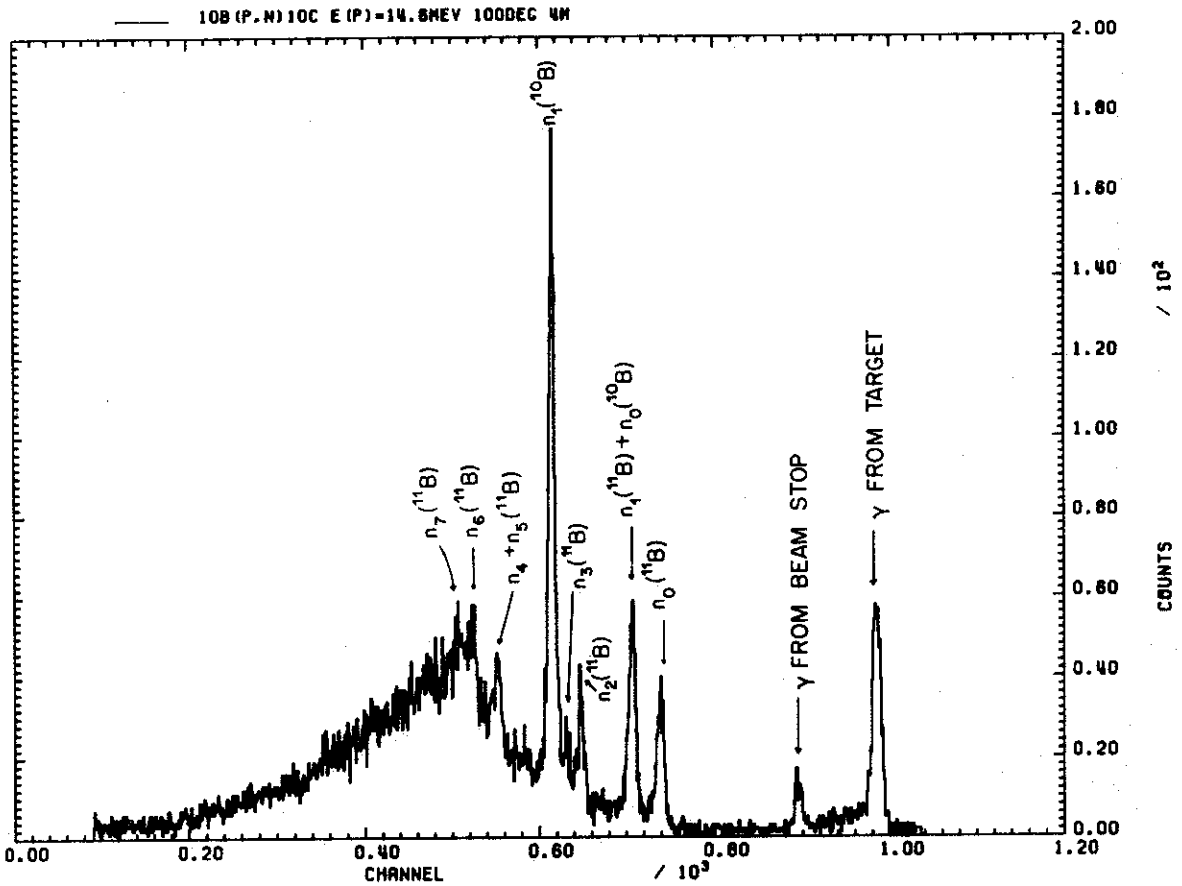
10B(P,N)10C E(P)=14.8MEV 100DEG UM
n1(10B)
n7(11B)
n6(11B)
n4+n5(11B)
n3(11B)
n2(11B)
n1(11B)+n0(10B)
n0(11B)
γ FROM BEAM STOP
γ FROM TARGET
COUNTS
/ 10²
CHANNEL
/ 10³
0.00
0.20
0.40
0.60
0.80
1.00
1.20
1.40
1.60
1.80
2.00

Fig. 2b

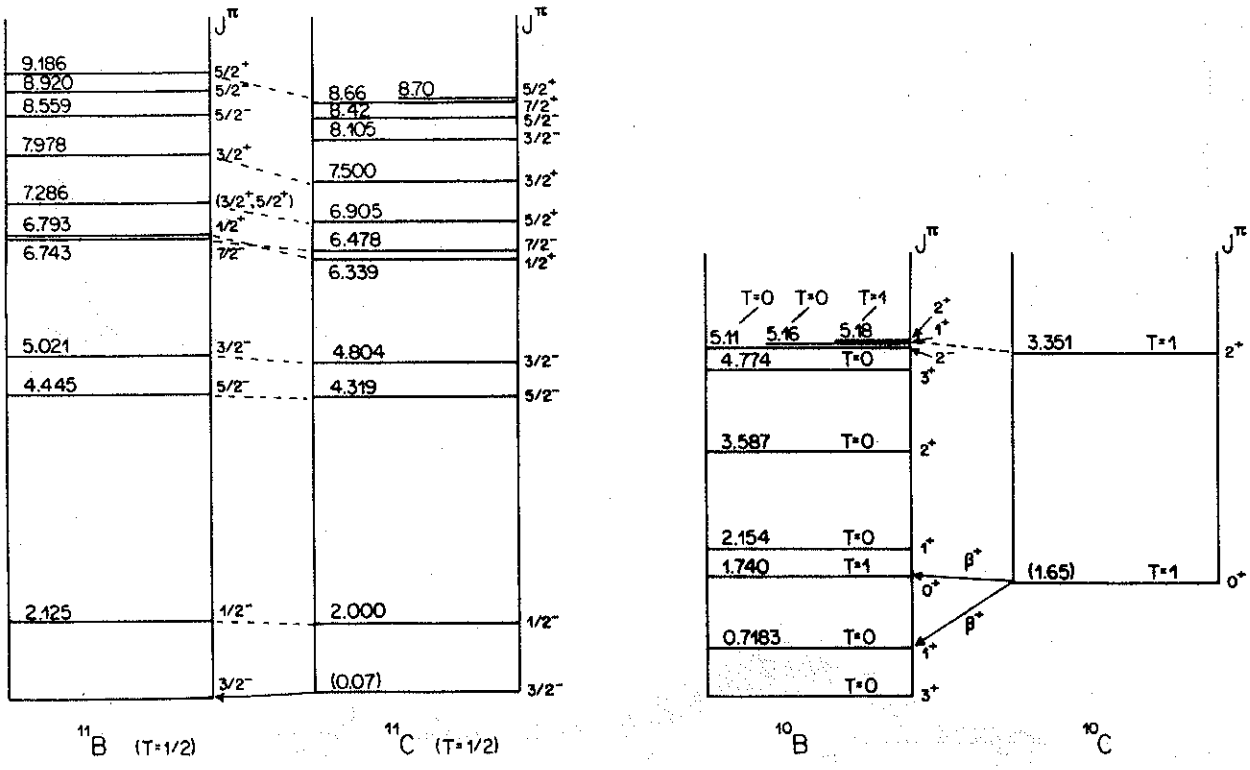
Jπ
9.186
8.920
8.559
7.978
7.286
6.793
6.743
5.021
4.445
2.125
5/2+
5/2+
5/2−
3/2+
(3/2+,5/2+)
1/2+
7/2−
3/2−
5/2−
1/2−
3/2−
8.66
8.70
8.42
8.105
7.500
6.905
6.478
6.339
4.804
4.319
2.000
(0.07)
5/2+
7/2+
5/2−
3/2−
3/2+
5/2+
7/2−
1/2+
3/2−
5/2−
1/2−
3/2−
11B (T=1/2)
11C (T=1/2)
T=0
T=0
T=1
5.11
5.16
5.18
4.774
3.587
2.154
1.740
0.7183
2+
1+
2−
3+
2+
1+
0+
1+
3+
β+
β+
3.351
(1.65)
2+
0+
10B
10C

Fig. 3

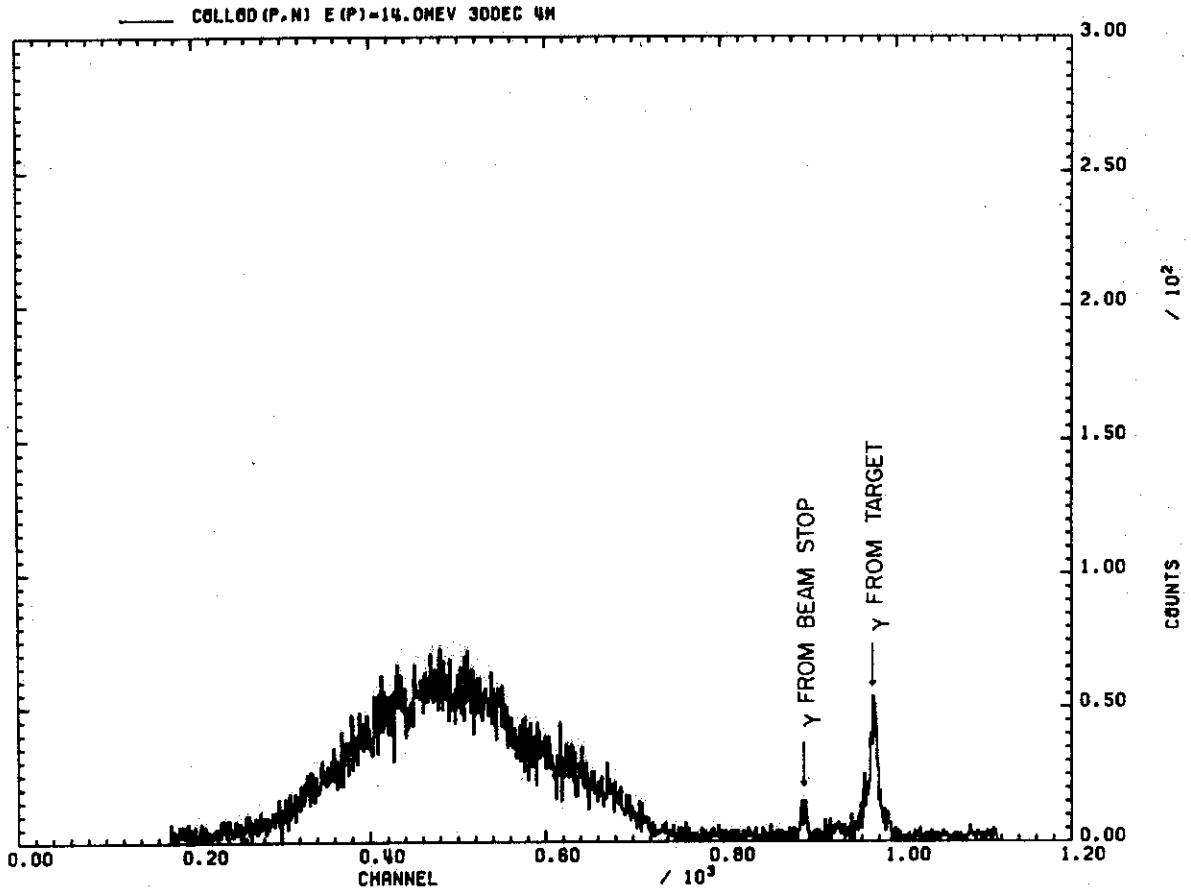
COLLOD(P,N) E(P)=14.0MEV 30DEG 4M
3.00
2.50
2.00
1.50
1.00
0.50
0.00
/ 10²
COUNTS
γ FROM BEAM STOP
γ FROM TARGET
0.00
0.20
0.40
0.60
0.80
1.00
1.20
CHANNEL
/ 10³

Fig. 4a

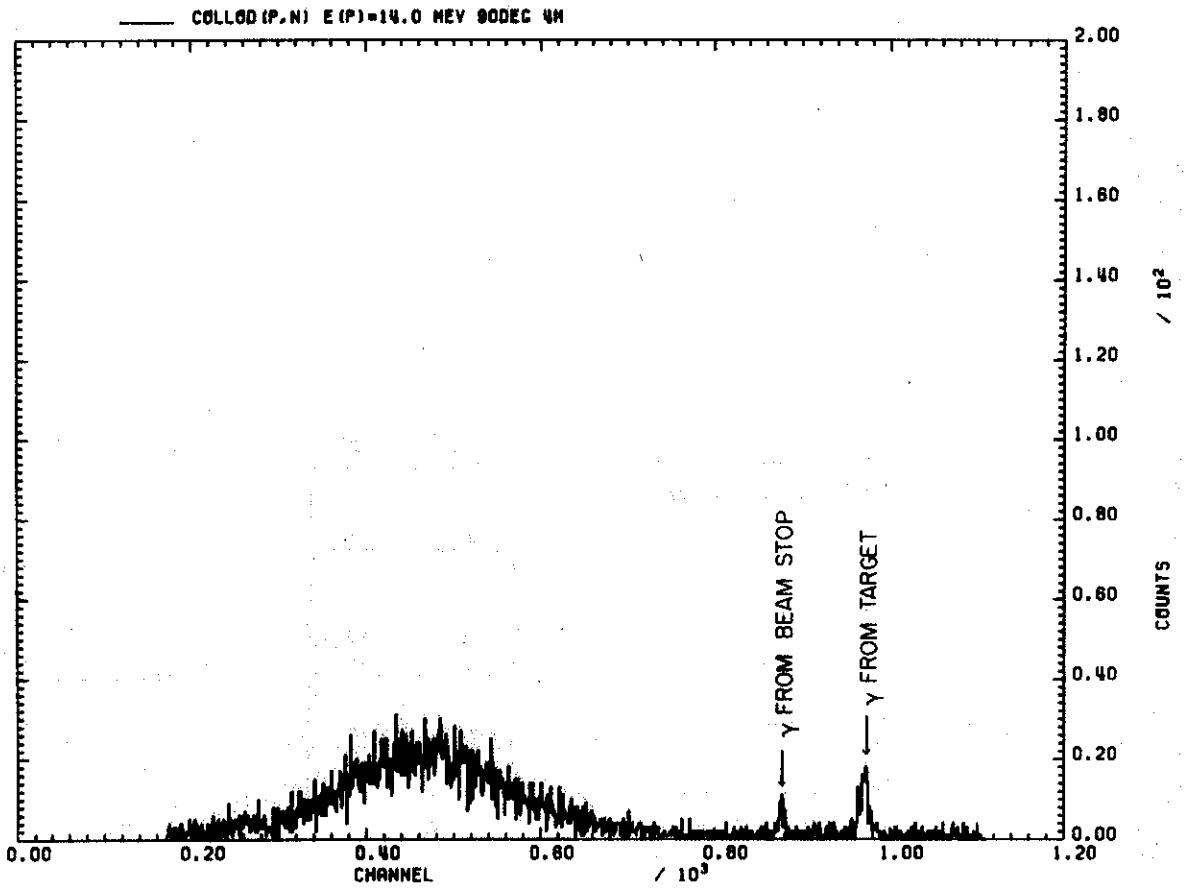
COLLOD(P,N) E(P)=14.0 MEV 90DEG 4M
2.00
1.80
1.60
1.40
1.20
1.00
0.80
0.60
0.40
0.20
0.00
/ 10²
COUNTS
γ FROM BEAM STOP
γ FROM TARGET
0.00
0.20
0.40
0.60
0.80
1.00
1.20
CHANNEL
/ 10³

Fig. 4b

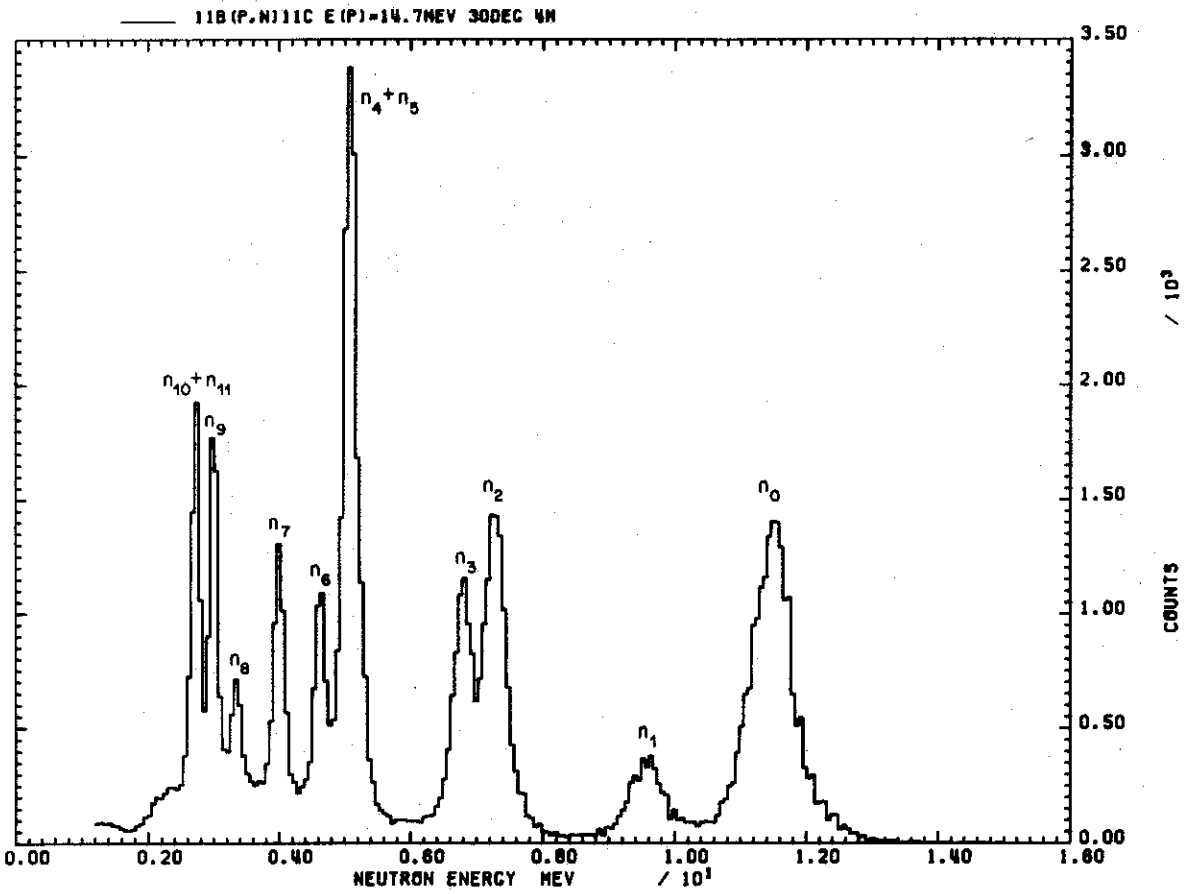
11B(P,N)11C E(P)=14.7MEV 30DEG 4M
n_4+n_5
$n_{10}+n_{11}$
n_9
n_8
n_7
n_6
n_3
n_2
n_1
n_0
COUNTS
/ 10^3
NEUTRON ENERGY MEV
/ 10^1

Fig. 5a

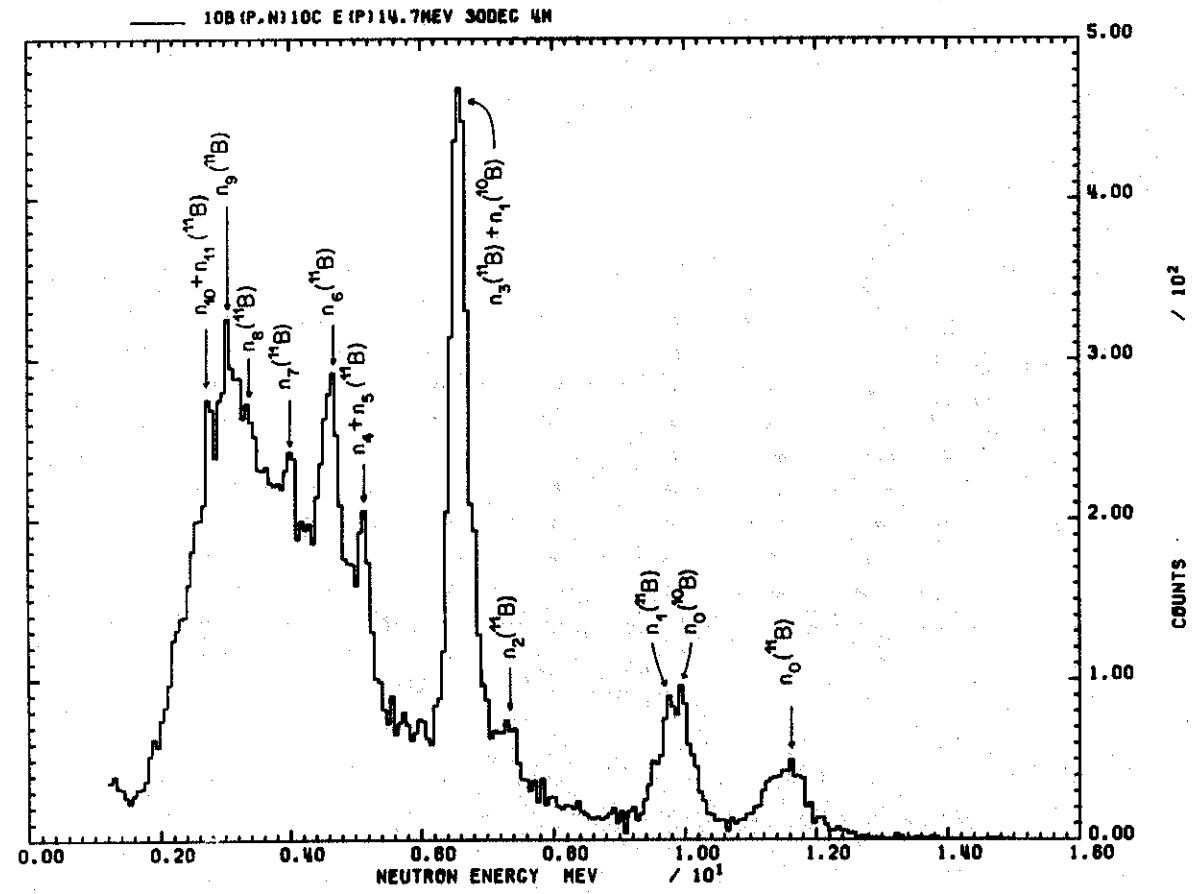
10B(P,N)10C E(P)14.7MEV 30DEC 4M
$n_{10}+n_{11}(^{11}B)$
$n_9(^{11}B)$
$n_8(^{11}B)$
$n_7(^{11}B)$
$n_6(^{11}B)$
$n_4+n_5(^{11}B)$
$n_3(^{11}B)+n_1(^{10}B)$
$n_2(^{11}B)$
$n_1(^{11}B)$
$n_0(^{10}B)$
$n_0(^{11}B)$
COUNTS
/ 10^2
NEUTRON ENERGY MEV
/ 10^1

Fig. 5b

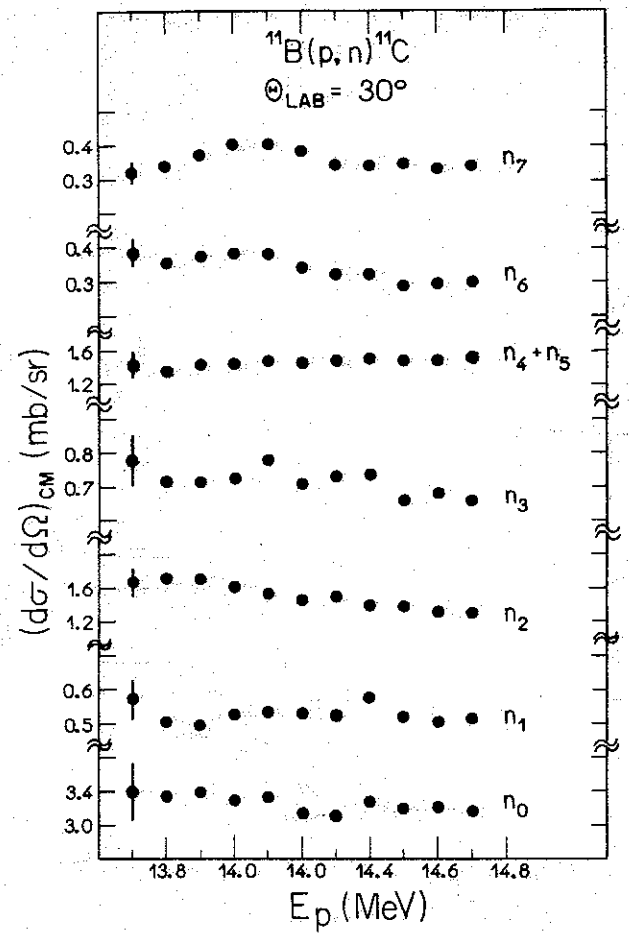
$^{11}B(p,n)^{11}C$
Θ_{LAB} = 30°
n_7
n_6
n_4+n_5
n_3
n_2
n_1
n_0
$(d\sigma/d\Omega)_{CM}$ (mb/sr)
E_p (MeV)

Fig. 6

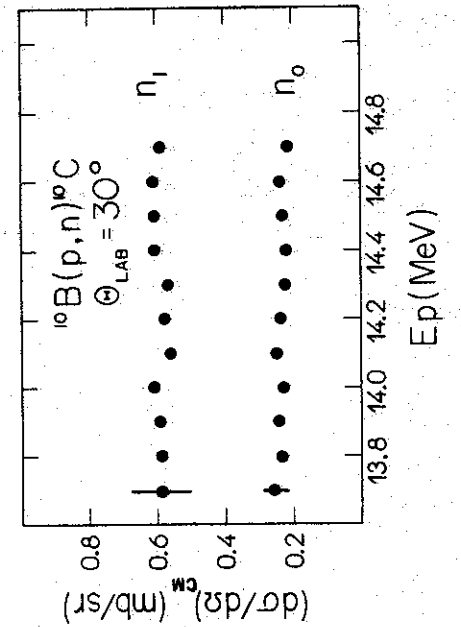
$^{10}B(p,n)^{10}C$
Θ_{LAB} = 30°
n_1
n_0
$(d\sigma/d\Omega)_{CM}$ (mb/sr)
Ep(MeV)

Fig. 7

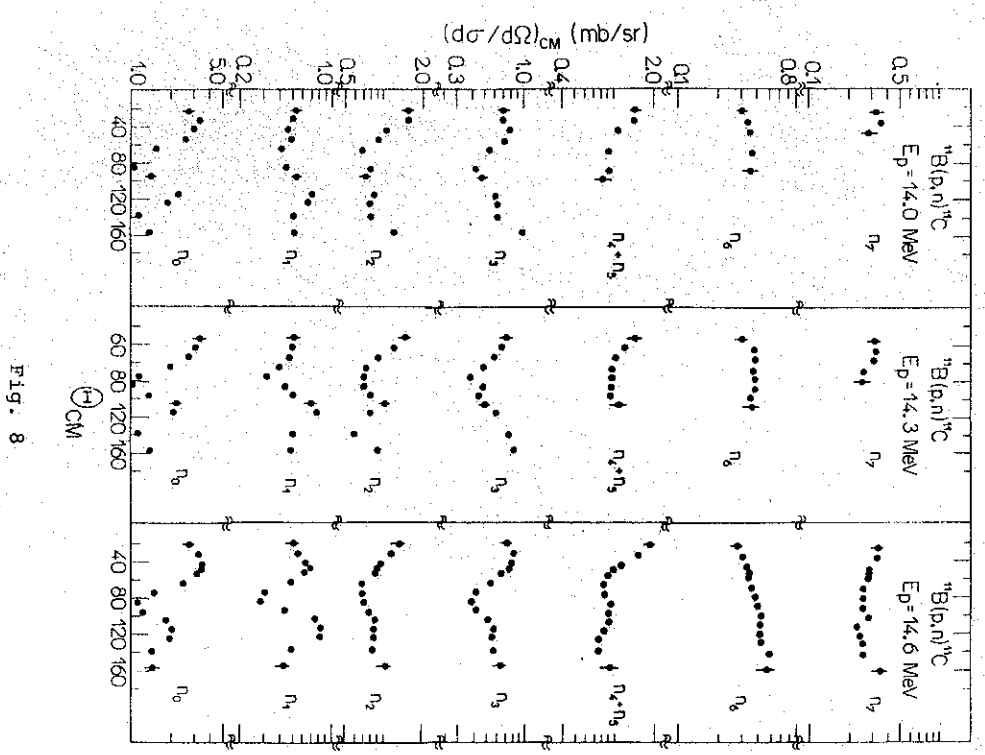
(dσ/dΩ)CM (mb/sr)
11B(p,n)11C
Ep=14.0 MeV
Ep=14.3 MeV
Ep=14.6 MeV
n0
n1
n2
n3
n4+n5
n6
n7
ΘCM

Fig. 8

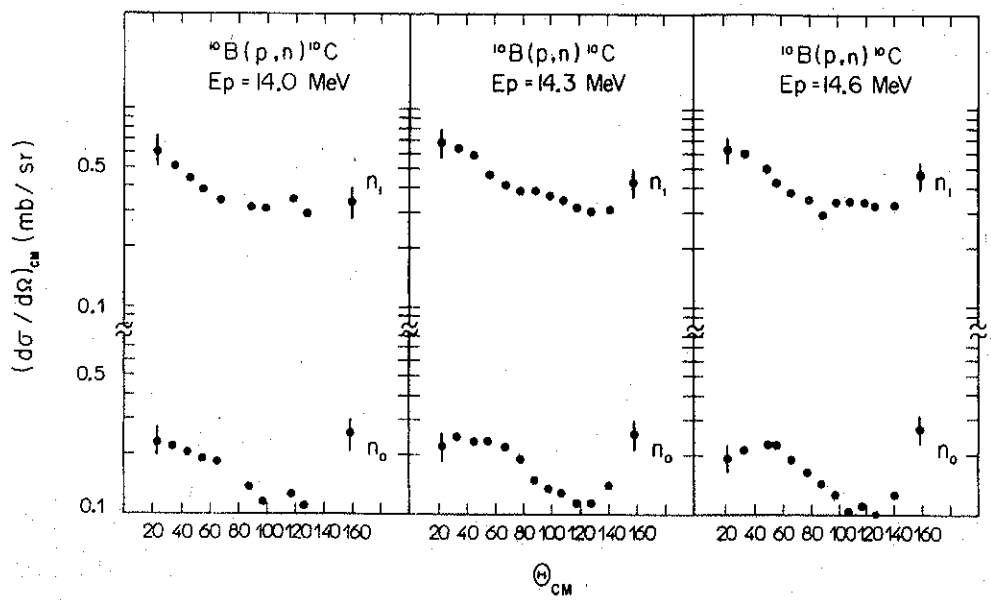
10B(p,n)10C
Ep = 14.0 MeV
Ep = 14.3 MeV
Ep = 14.6 MeV
(dσ/dΩ)CM (mb/sr)
n1
n0
ΘCM

Fig. 9